

Article

Combination of Tree Configuration with Street Configuration for Thermal Comfort Optimization under Extreme Summer Conditions in the Urban Center of Shantou City, China

Bohong Zheng ¹, Komi Bernard BEDRA ¹, Jian Zheng ^{2,*}  and Guoguang Wang ^{2,3}

¹ School of Architecture and Art, Central South University, Changsha 410083, China; zhengbohong@csu.edu.cn (B.Z.); komibedra@csu.edu.cn (K.B.B.)

² School of Architecture, South China University of Technology, Guangzhou 510641, China; wgg999@126.com

³ State Key Laboratory of Subtropical Building Science, South China University of Technology, Guangzhou 510641, China

* Correspondence: arzhengjian@mail.scut.edu.cn

Received: 5 October 2018; Accepted: 11 November 2018; Published: 14 November 2018



Abstract: Along with global climate change and the worldwide heat island phenomenon, developing climatic methods and planning practices for the benefit of thermal comfort is of increasing interest. Studies have focused on urban streets, studying the aspect ratio, the orientation, street vegetation patterns, etc. and how they affect thermal comfort. While the role of vegetation is undeniable, this paper asks the question whether the effects of a tree configuration does not vary under different street configurations, and if yes, how to select tree species and determine their appropriate layout. Here, an analytical framework is proposed to test the different tree configurations (changing one variable at a time) with the least favorable street configuration. It is confirmed that the east–west oriented streets are the least favorable cases and denser tree canopies are better for cooling. The interval between the trees are observed to have an optimal effect when it is equal to the crown width at maturity. Furthermore, the results show that the heat mitigation rate of a tree configuration is not linearly improved by the Aspect Ratio (AR). In the case of Shantou city, the improvement of thermal comfort slows down when the AR reaches 1.5 while *Mangifera indica* planted with 10 m intervals is recommended among the common street-tree species. Other species could be used also, but should meet the requirements of the canopy density and the interval of layout. The paper does not consider other configuration options such as asymmetrical cases of street geometry and one-side or axial tree planting, etc., but the framework allows for adding such options and simulating thermal comfort for a greater number of scenarios.

Keywords: tree configuration; street configuration; heat mitigation; thermal comfort; summer

1. Introduction

Worldwide rapid urbanization and the corresponding shift from the natural environment to a densely built-up environment has raised many issues, among which city-induced climate change, especially the urban heat island phenomenon has stimulated much research interest [1]. High air temperature more and more recorded in urban outdoor spaces affects human thermal comfort at pedestrian level and public health [2,3]. Focusing on the climatic condition at the street level, it has been well-established that a street orientation and its Aspect Ratio (AR) both influence the pedestrian comfort [4–6]. The aspect ratio is defined as the ratio between the average height of the buildings along a street canyon and the width of the street. The street canyon is considered uniform if its aspect

ratio is approximately equal to 1, shallow if the aspect ratio is below 0.5 and deep if it equals 2 or more [4]. Some authors refer to the combination of these two parameters (orientation and aspect ratio) as the street configuration [7]. The effects of street configurations on human thermal comfort have been studied by various scholars [6,8–10] resulting mostly in recommendations to consider through the design process. Thermal comfort is achieved when the condition of mind expresses satisfaction with the thermal environment [11]. Thermal comfort optimization is often mentioned by various authors [12,13] as to signify the specific measures taken under difficult thermal conditions to improve that condition of mind and get it as close as possible to total satisfaction for the average user.

In the cases of street configurations inducing intense heat stress during summer time, street tree planting is one of the most frequent solutions recommended by various studies as a tool for optimizing thermal comfort [8,14] and reducing health-related consequences of increased air temperatures [15,16]. According to numerous studies, by providing shade on the ground, trees modify the microclimate by altering the solar radiation and terrestrial radiation [17], thus reducing the air temperature and mitigating urban heat islands [18]. For instance, Abakri et al. [19] argued that urban trees by protecting buildings from direct sunlight during summer reduce the air-conditioning demand and by evapotranspiration reduce the air temperature. By using a simplified comfort evaluation elaborated with the energy budget method, X. Picot [20] showed that the shading effect of trees can reduce the radiation human bodies are exposed to and generate an energy budget very close to comfort (under 50 W/m^2). The cooling effect of trees was confirmed also by comparing field measurements of two typical urban buildings in Akure, Nigeria. Indoor–outdoor temperature differences show a peak of $5.4 \text{ }^\circ\text{C}$ for the un-shaded building, while it did not exceed $2.4 \text{ }^\circ\text{C}$ for the shaded building. An extensive literature on thermal effects of urban greening is provided by E. Jamei et al. [21].

What tree configuration (type and layout) is necessary and adapted to which street configuration, is a question that fewer studies have focused on. The effect of the tree density (dense and light-dense) on the air temperature at street level has been studied when the trees are planted on north–south and east–west orientated symmetrical streets, with $\text{AR} = 1$ and $\text{AR} = 2$ considering perpendicular and parallel winds [22]; dense trees are shown to provide the lowest air temperature with $\text{AR} = 2$ and parallel winds. The effect of the tree configuration (alignment and orientation) on thermal comfort around buildings has been studied also comparing three vegetation patterns (grass, shrub and trees) [23]; the study showed that even though trees have a decreasing effect on wind speed, they are more efficient at improving thermal comfort than grass and shrub. Shashua-Bar et al. [24,25] based on in-situ measurements, investigated the tree canopy coverage along with four other variables (traffic load, surface albedo, street deepening aspect and ventilation). They estimated the thermal effect of each variable on air temperature in order to gauge their importance and relevance in affecting microclimate for the purpose of designing effective passive cooling scenarios. E. Andreou [26] by simulating case models examined the effects of street geometry, orientation, wind speed surface albedo and trees on urban canyon microclimate. Each of the parameter values were examined differently. In particular, 5 m large trees were considered in the case models and the study showed that they have a much more considerable effect on east–west streets and the heat mitigation is more significant for the side of the street facing south. Coutts et al. [27] also studied the effect of two contrasting tree canopy density (high and low) in east–west oriented streets with two contrasting canyons form (deep and shallow). The field measurements in summer and the thermal comfort estimations revealed that the maximum daytime cooling reached $1.5 \text{ }^\circ\text{C}$ in the shallow canyon while the effect of the street trees where masked by the shading effect of tall buildings. Many other studies likewise showed the role of street trees on thermal comfort at pedestrian level; an extensive literature is provided in the works of Jamei et al. [23] and Bowler et al. [28].

Even though the effects of street trees on improving thermal comfort at street level has been studied by the above-mentioned works, either by comparing their effects with those of other urban street variables or analyzing the effects of trees combined with some other variables, the effects of the combination of tree configurations with street configurations were not examined systematically.

The scenarios models did not fully consider all combinations of the targeted values of the variables to analyze all possible thermal comfort outcomes. Even though more combinations are possible with automatic algorithms developed for evaluating and simulating the improvement of outdoor comfort, still, on the one hand, the effect of building geometry and human body location are analyzed without tree as input variable [29] and on the other hand, tree location is analyzed on street and parking lots without street configuration as variable [30]. Many of the works mentioned in the previous paragraph showed at least that the effect of trees can vary in different cases of street orientation or aspect ratio. If so, how to select the appropriate tree species and determine their appropriate layout to ensure an optimal thermal comfort on a wide range of streets? For practical urban design purposes, this is the main question that this paper is intended to answer by systematically creating scenarios and analyzing their thermal comfort outputs.

In recent studies human thermal comfort indexes such as Predicted Mean Vote (PMV) and Percentage Person Dissatisfied (PPD) [31], Physiologically Equivalent Temperature (PET) [32], modified Psychologically Equivalent Temperature (mPET) [33], Standard Effective Temperature (SET) [34], Universal Thermal Climate Index (UTCI) [35], etc., are widely used for assessing and predicting outdoor thermal comfort. In this paper, two user-friendly and widely used energy balance models (RayMan [36,37] and Envi-met [38]) will be used to estimate PMV and PET for various combinations of street and tree configurations. In order to help select the proper tree species and optimize their layout in respect of the street configuration, here will be introduced an analytic framework, applied to Shantou city, China. First, the meteorological data of Shantou city will be studied in order to appropriately select the simulation date and the corresponding weather data. Second, the analytical framework, which comprises two main parts, will first investigate the existing street configurations in the study area, then estimate the thermal comfort for different tree configurations in the worst street configuration cases. Third, in a result analysis, the estimated thermal comfort for the different scenarios will help examine the effects of the canopy density and the layout interval under different aspect ratios. The optimal configurations options will be detected to provide a guideline for urban street design.

2. Material and Methods

This section describes the methodology and its testing with “the small park” in Shantou city (which will be briefly presented in the Section 2.1 through an overview of its geography and its importance as thermal comfort is concerned). Here the methodology, briefly, consists of simulating thermal comfort for defined street and tree configuration scenarios and analyzing the impacts of each parameter on the overall thermal comfort output. To perform this task, this study adopts RayMan and ENVI-met, two broadly and reliably used models for this kind of simulation. Basically, the boundary conditions needed for the simulations with these two software models are: temperature, relative humidity, wind speed (and wind direction for ENVI-met). The Section 2.2, shows the analysis of the climatic data which will help select the simulation date and the necessary boundary conditions. The thermal comfort estimation method is explained in the Section 2.3—an overview of the physiological heat stress on the simulation date is also given. The whole framework for analyzing tree and street configurations and their impacts on outdoor thermal comfort during summer time is fully described in the Section 2.4, where the simulations’ process is divided into two main steps: first for different combinations of street orientations and aspect ratios, second for different tree configurations used under the worst street configuration scenario. The outputs should help, on the one hand, understand how different tree parameters such as canopy density and layout behave in different Orientation and Aspect Ratio cases, and on the other hand, detect the optimal configurations for thermal comfort. For the purpose of testing the framework but also for effecting realistic outputs, all the street orientations and aspect ratios and the tree models used for the simulations are derived from the investigation of the study area.

2.1. Study Area

Shantou is located in eastern Guangdong with latitude spanning $23^{\circ}02'33''$ – $23^{\circ}38'50''$ N and longitude $116^{\circ}14'40''$ – $117^{\circ}19'35''$ E. The city is located at the mouths of the Han, Rong, and Lian Rivers. Shantou is a prefecture-level city on the eastern coast of Guangdong, China, with a total population of 5,504,600 and an administrative area of 2.199 km² [39]. Shantou is a significant city in the Chinese 19th-century history as one of the treaty ports established for Western trade and contact. The city also was one of the original special economic zones of China established in the 1980s.

Xiaogongyuan, “the small park”—which is the specific study area in this paper—is located in the old urban center of Shantou (Figure 1). “Small Park” was the commercial center of the city; it is the core landmark and the cultural symbol of the old urban area. Here, it is chosen as the study area because of its touristic importance for Shantou city, as pedestrian outdoor comfort is an important concern for touristic sites.

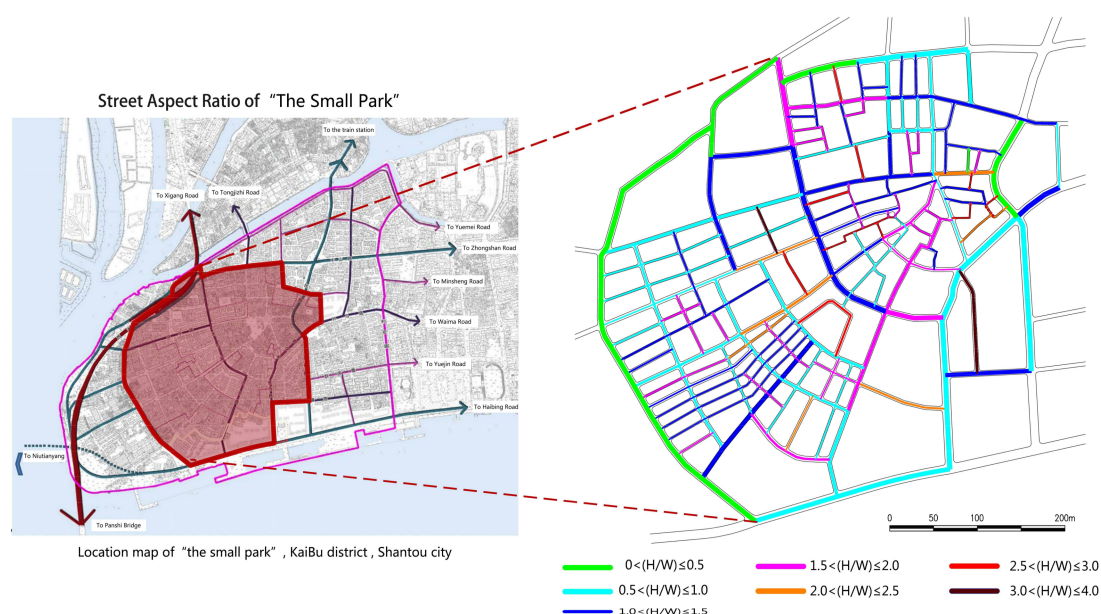


Figure 1. Study area (“the small park”, Shantou city) and streets’ classification by aspect ratio.

According to the Köppen climate classification [40,41], Shantou has a humid subtropical climate with short, mild, warm winters, and long, hot, humid summers. Winter begins sunny and dry but becomes progressively wetter and cloudier. Spring is generally overcast, while summer brings the heaviest rains of the year though it is much sunnier; there are 8.2 days annually with 50 mm of rainfall. Autumn is sunny and dry. The monthly 24-h average temperature ranges from 14.7 °C in January to 29.23 °C in July, and the annual mean is 21.53 °C. The annual rainfall is around 1618 mm, about 60% of which occurs from May to August, with monthly percent possible sunshine ranging from 28% in March to 58% in July and October, the city receives 1979 h of bright sunshine annually [42].

2.2. Data

Meteorological data used in this study, are collected from the China standard climate monitoring station No 59316 located in Shantou city ($23^{\circ}23'$ N; $116^{\circ}41'$ E; 2.3 m above sea level) [43]. First, daily averages of air temperature, relative humidity, wind speed, and wind direction are collected for the years 2008 to 2017 to identify the hottest summer conditions over the past ten years. For this purpose, the monthly average temperatures were computed for four months (June to September). As shown in Figure 2, even though the hottest month varies along the years, the hottest temperatures were registered in July 2014 and July 2016 when the average temperatures were, respectively, 30.32 °C and 30.40 °C. The Figure 3 shows the daily average temperature of July 2016; the 8 July 2016 is identified as

the hottest day of that month. Since the comfort optimization—which is the concern of this paper—will be analyzed by simulating human comfort under different scenarios, the hourly weather data of the 8 July 2016 will be used to test the efficiency of each scenario. Second, the hourly averages of air temperature, relative humidity, wind speed of the hottest day (summarized in Figure 4) are analyzed in order to select the boundary conditions of the simulations.

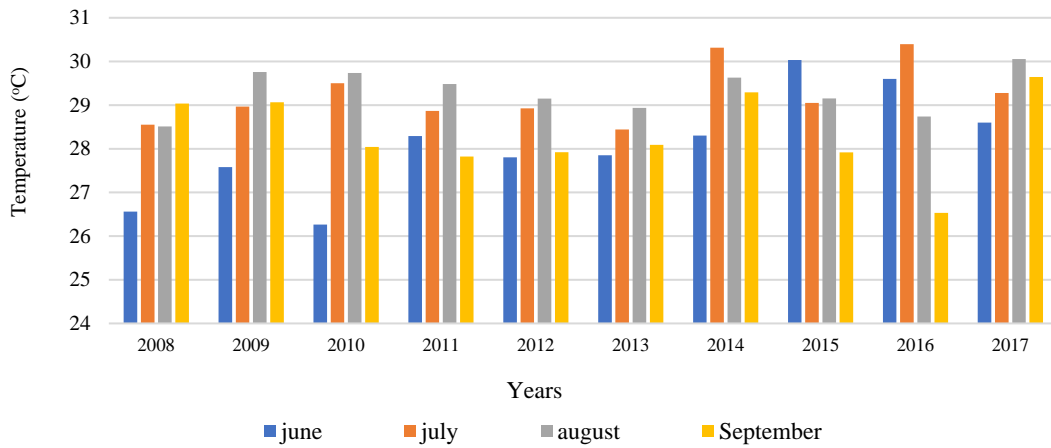


Figure 2. Monthly average temperature during summer (2008–2017).

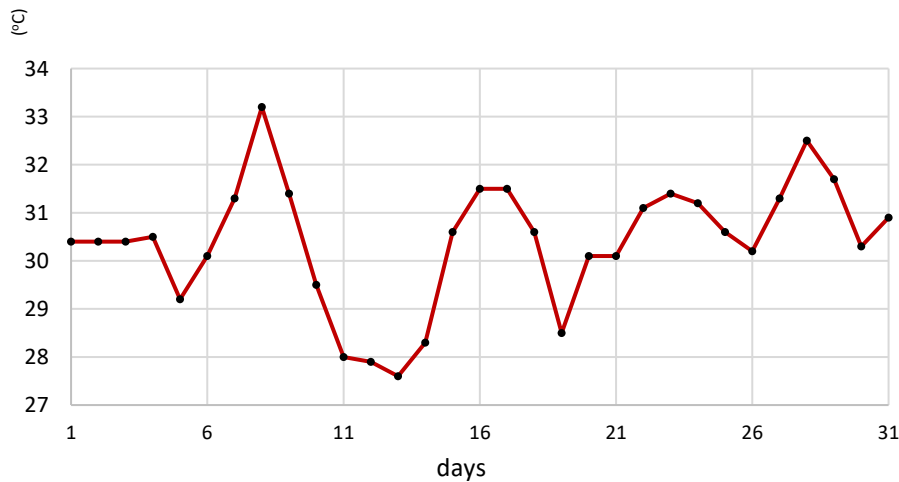


Figure 3. Daily average temperature in July 2016.

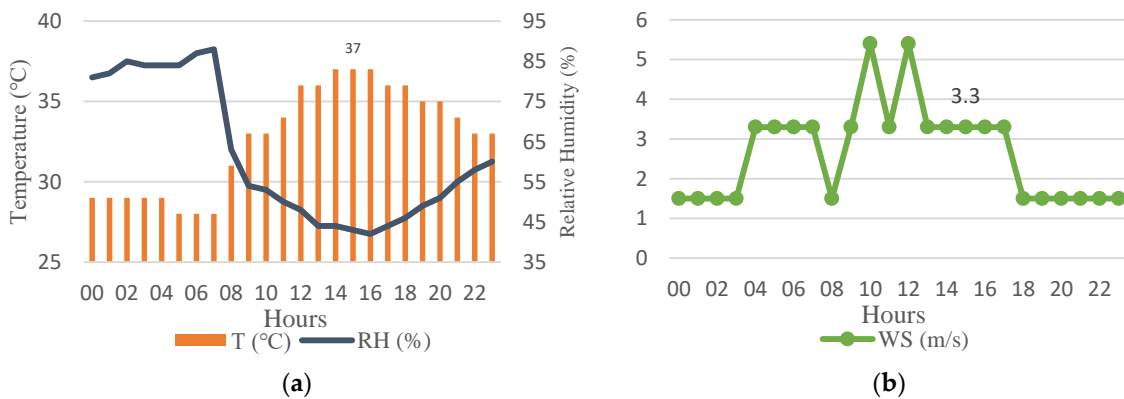


Figure 4. Air Temperature (T), Relative Humidity (RH) and Wind Speed (WS) on the 8 July 2016. (a) Temperature and relative humidity; (b) Wind speed.

2.3. Thermal Comfort Evaluation

The energy balance of the human body is a modern method that enables to derive thermal indexes and is able to describe and quantify the effects of the thermal environment on human beings [44,45]. To estimate the energy balance, various models were developed, which usually consider many meteorological parameters, surface albedo and solid angle proportion [46–49]. There are a variety of comfort indexes widely used for estimating human thermal comfort: PMV, PPD, PET, mPET, SET, UTCI, etc. In recent studies, PMV and PET are widely used for assessing and predicting outdoor thermal comfort. PMV and PET both include the mean radiant temperature (T_{mrt}), which is—especially during sunny weathers—the most important input parameter for the energy balance [48]. In this study, PET and PMV will be jointly used to predict human thermal comfort for the various scenarios. Two models (RayMan and Envi-met) are chosen, for their user-friendliness and the fact that they are reliably used by many recent studies to assess and predict human thermal comfort [50–53].

To have an overview of the thermal comfort provided by natural conditions on the 8th July 2016, PET and PMV are estimated with RayMan Pro, using the above temperature, relative humidity and wind speed data as input. Geographic data are set as provided by the monitoring station No 59316: geographic longitude ($116^{\circ}41' E$), geographic latitude ($23^{\circ}23' N$), and altitude (2.3 m). Personal data are set according to the “Standard Human” defined by the International Organization for Standardization (ISO) 7730 [54]: height (1.75 m), weight (75 kg), age (35), and sex (male). The clothing insulation is set as 0.5 clo, corresponding to a summer clothing; the activity level as 80 W, corresponding to a walking activity at 0.5 m/s (ISO 7730). The results are shown in the Figure 5 where the PMV values indicate that the threshold of heat stress (+3) when the psychological sensation could be described as very hot [54] has been surpassed between 9:00 and 19:00. The PET values went above $41^{\circ}C$, which is the threshold value for “extreme heat stress” in the classification of Matzarakis A. and Mayer H. [55]. It is also noted that the highest air temperatures are reached between 14:00 and 16:00, and the most uncomfortable hours are 15:00 and 16:00 (where the PMV values equal +5.5). These observations will determine the simulation times, defined in the next section.

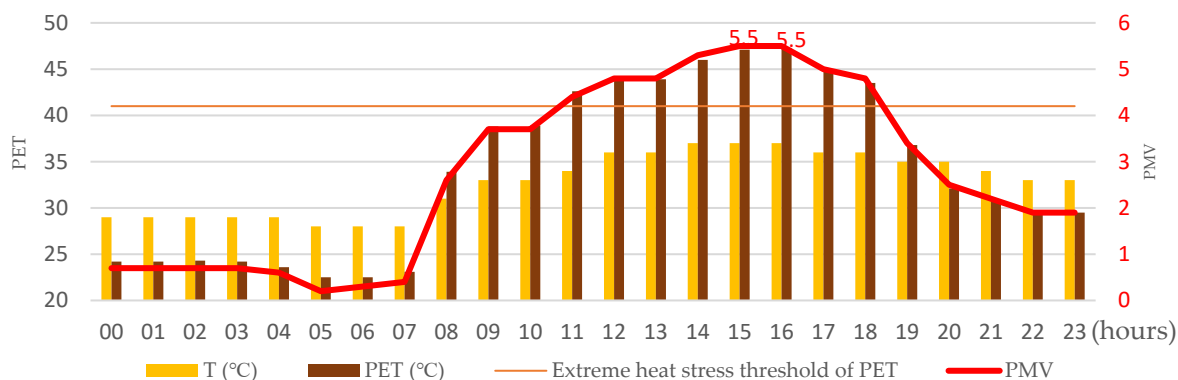


Figure 5. Thermal comfort level on the 8th July 2016.

2.4. Tree and Street Configuration Analytical Framework

In order to figure out the optimal combinations of tree and street configurations, this paper proposes an analytic framework (Figure 6) that will help simulate thermal comfort for a variety of Street Configuration (SC)–Tree Configuration (TC) scenarios. The analytical framework is segmented into two main steps:

- (i) a Spatial–Temporal Comfort Diagnosis (STCD) that simulates thermal comfort for as many SC scenarios as identified in the study area, and diagnose the problematic scenarios;
- (ii) a Street Thermal Comfort Optimization (STCO) where the problematic SC scenarios are combined with TC scenarios to determine the optimal options for pedestrian outdoor comfort.

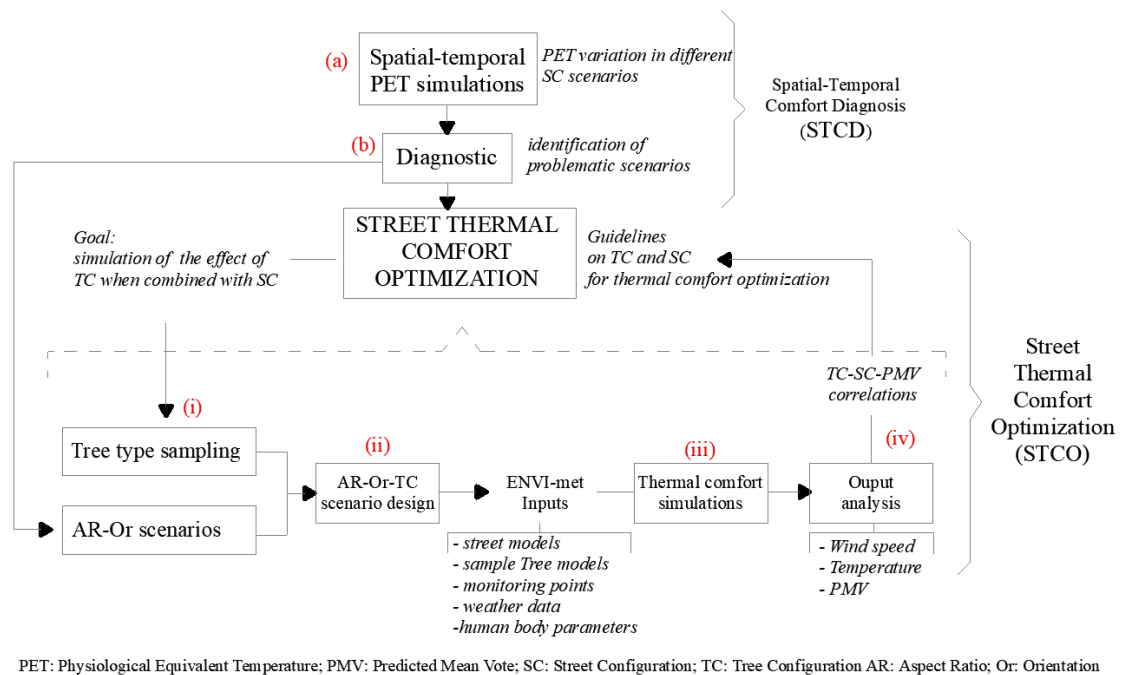


Figure 6. Tree and street configuration analytical framework.

2.4.1. Spatial–Temporal Comfort Diagnosis (STCD)

Spatial–Temporal PET Simulations (a)

The STCD consists of simulating PET for a matrix of street AR and Orientation (Or) combinations existing in the study area, in order to read the variations of comfort level in time (in this case from 9:00 to 19:00) and in space (at 5 points positioned in the middle of each street). PET is used here because its values are expressed in °C, which are easier to read.

Street Configurations (Or/AR) are identified in the study area with seven AR values (0.5; 1.0; 1.5; 2.0; 2.5; 3.0; and 4.0) for four approximate Orientations: North–South (N–S); East–West (E–W); Northeast–Southwest (NE–SW), and Northwest–Southeast (NW–SE). In the (7 × 4) matrix of Or/AR cases, four cases are non-existent in the study area, which leaves us with 24 identified combinations (see Table 1).

Table 1. Identified Or/AR cases in the study area.

	AR = 0.5	AR = 1.0	AR = 1.5	AR = 2.0	AR = 2.5	AR = 3.0	AR = 4.0
N-S	●	●	●	●	○	●	●
EW	●	●	●	●	●	●	○
NE-SW	●	●	●	●	●	○	○
NW-SE	●	●	●	●	●	●	●

● Existent; ○ non-existent.

To perform the STCD, RayMan Pro version 3.1 Beta (Andreas Matzarakis, Research Center Human Biometeorology, Freiburg, Germany) is used to calculate PET for the 24 Or/AR cases. PET is calculated on the basis of two main inputs: the 24 streets’ 3D models defined by the different Or/AR cases (see Figure 7), and the weather datafile (Table 2). To build the street models, the default street width is set as 10m and the heights are determined by the AR values. The five monitoring points put in the model are named A, B, C, D, and E, positioned either in a top-down or in a left-right order depending on the street orientation (see Figure 7). Geographic and personal data are set as described in the Section 2.3.

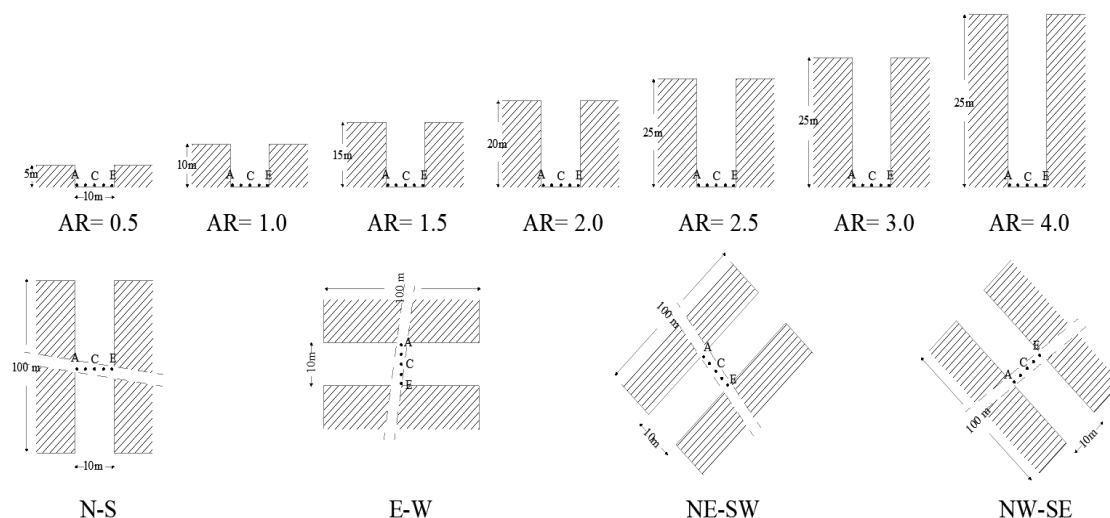


Figure 7. Aspect Ratios and Orientations identified in the study area.

Table 2. Air Temperature (Ta), wind velocity (v), and Relative Humidity (RH) datafile as RayMan Pro input.

Date (Day.Month.Year)	Time	Ta (°C)	v (m/s)	RH (%)
8.7.2016	9:00	33	3.3	54
8.7.2016	10:00	33	5.4	53
8.7.2016	11:00	34	3.3	50
8.7.2016	12:00	36	5.4	48
8.7.2016	13:00	36	3.3	44
8.7.2016	14:00	37	3.3	44
8.7.2016	15:00	37	3.3	43
8.7.2016	16:00	37	3.3	42
8.7.2016	17:00	36	3.3	44
8.7.2016	18:00	36	1.5	46
8.7.2016	19:00	35	1.5	49

Data source: China standard climate monitoring station No 59316 (Shantou city).

The Diagnosis (b)

The matrix of PETs (Figure 8), generated in Microsoft Excel version 15.0 (Microsoft Corporation, Redmond, WA, USA) is a spatial-temporal classification of the PET values obtained by the above-described calculations at each of the points A, B, C, D, E and at different times of the day (9:00–19:00). The spatial-temporal tables are then organized by the aspect ratio and the orientation of the streets models where the points are located. To make the matrix easy to read, the PET values have replaced by color-values on a scale of 30 °C to 50 °C (see legend).

The matrix shows a general heat stress between 30 °C and 50 °C—which is uncomfortable [56]—independently of the Aspect Ratio and the Orientation. This confirms the extreme thermal condition of the simulation day. Nevertheless, it can be noticed, on the one hand, that under the same orientation, the higher the aspect ratio is, the more the heat stress is mitigated. On the other hand, among the four street orientations, the E–W is the hottest and the aspect ratio augmentation on such streets does not show so much of heat stress mitigation. Globally, this observation is explained by the fact that solar access is higher at lower aspect ratios and the sun shine duration is longer for E–W oriented streets [57]. Through the comparison of PET values across different orientations and aspect ratios, it can be diagnosed that under a globally uncomfortable heat stress, that E–W orientated streets are more problematic and the lower the aspect ratio is, the hotter the street is. As often recommended in such situations, street tree should be used to reduce the thermal discomfort on the streets.

Next, Tree Configuration (typology and layout) will be studied taking E–W oriented streets as reference to test the efficiency of different tree types and layouts at mitigating thermal discomfort. Since successive aspect ratios (for E–W oriented streets) do not show very significant variations in PET matrixes, only three AR values will be considered in building the test scenarios: AR = 0.5, AR = 1.5, and AR = 3.

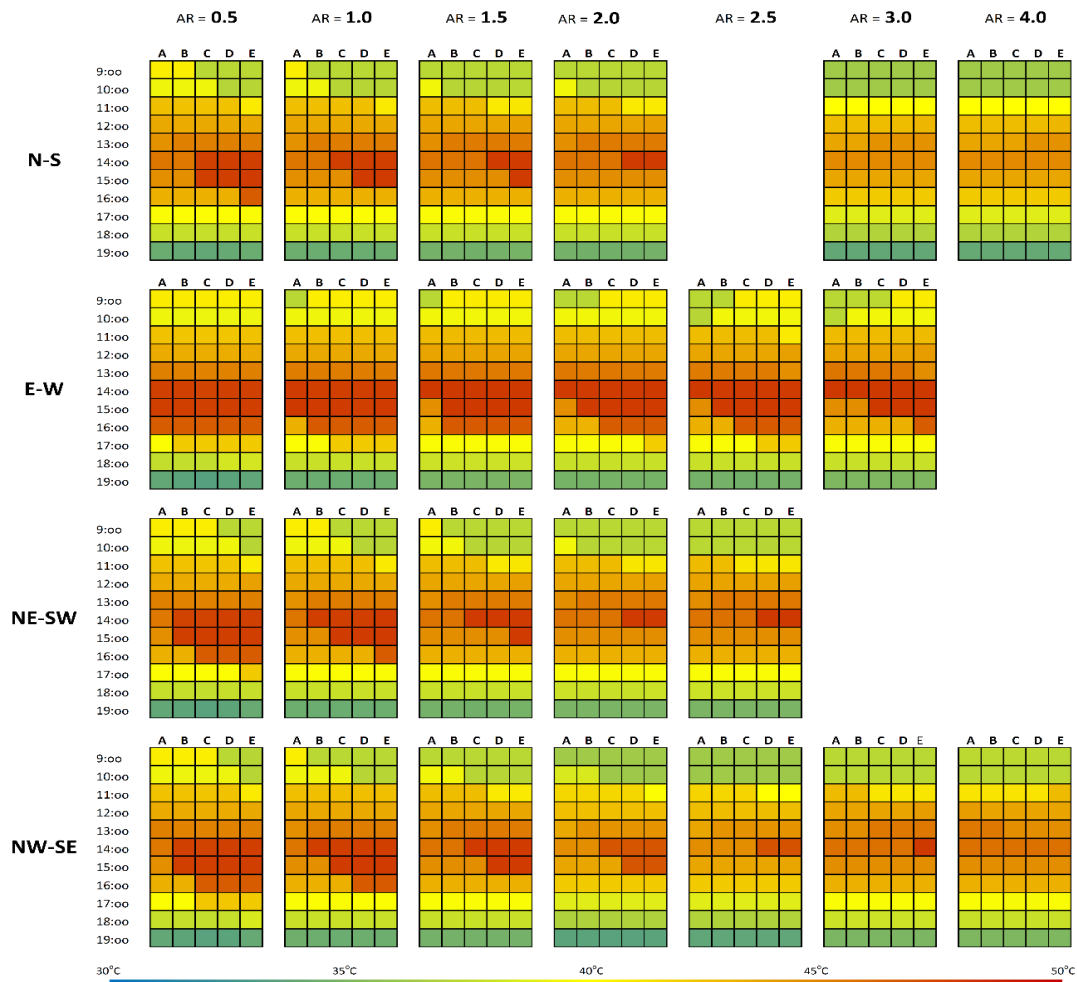


Figure 8. PET matrix for the existing street configurations in the study area.

2.4.2. Street Thermal Comfort Optimization

The STCO analysis is done in four steps including: (i) tree type sampling, (ii) Or/AR/TC scenario design, (iii) thermal comfort simulation, (iv) output analysis and street tree guidelines.

Tree Type Sampling (i)

For the purpose of demonstrating the analytical process proposed in this paper, the tree sampling is done on the basis of an investigation of the commonly used species as street trees in Shantou city [58]. The tree types are defined here by their heights, crown widths, canopy densities and shapes at maturity. These parameters have been investigated and presented in Table 3.

Since the trees' sizes are very variable depending on their age, their location, etc., in this paper, the sampling considers the minimum dimensions at maturity to ensure that the simulated shading of the selected species are not exaggerated.

Because the cooling effect of trees is determined merely by the proportion of shade they provide on the ground (Leaf Area Density or Tree Area Density) [59–61], the sampling will first select the

representative canopy densities—which are mostly three types in this case: dense, medium, and open. For each canopy density, the available biggest minimum size at maturity is considered for an optimum shade on the streets. Therefore, three tree species (Ti) are selected as samples: mangifera indica (T1), Alstonia scholaris (T2), and Bombax Ceita (T3).

Table 3. Common tree species for street tree in Shantou city.

Tree Species	Canopy Density	Height at Maturity (m)		Crown Width at Maturity (m)		Shape
		Min–Max	Average	Min–Max	Average	
Cinnamomum burmannii	dense	1.3–19	5	0.1–23.5	3.5	triangular
Aleurites moluccana	dense	10–20	9	6	-	spreading
Mangifera indica (T1)	dense	15–23	-	10–15	10	round
Delonix regia	medium	10–12	-	12–18	-	T-shape
Acer x freemanii Jeffersred	medium	10–45	16	9–12	11	oval
Alstonia scholaris (T2)	medium	17–40	30	10	-	spreading
Eucalyptus tereticornis	moderate	25–50	25	7–30	16	columnar
Prunus dulcis	open	5–8	-	5–8	-	vase
Bombax Ceita (T3)	open	15–23	-	10–15	5	Oval

Or/AR/TC Scenario Design (ii)

The Orientation/Aspect Ratio/Tree Configuration (Or/AR/TC) scenarios are designed by combining the four parameters in a tree-shape order. The E–W orientation (the worst orientation defined by the STCD) is first combined with three aspect ratios (0.5; 2.5; and 3.0). The three Or/Ari scenarios are combined with Tree Configurations—defined by the type of tree (Ti) and the interval between the trees (di). The three sample trees are tested for di = 5 m, 10 m, and 15 m, which gives 9 tree configurations for each Or/AR case, and 27 scenarios for the all 3 Or/AR cases (see Table 4).

Table 4. Orientation-aspect ratio-tree configuration (Or/AR/TC) scenarios.

ORIENTATION (Or)	Or/ARi	Or/ARi/Ti	Or/ARi/Ti/di
	Ari = 0.5; 1.5; 3.0	Ti = T1; T2; T3	di = 05 m; 10 m; 15 m
E–W	E–W/0.5	E–W/0.5/T1	E–W/0.5/T1/05
			E–W/0.5/T1/10
			E–W/0.5/T1/15
	E–W/0.5	E–W/0.5/T2	E–W/0.5/T2/05
			E–W/0.5/T2/10
			E–W/0.5/T2/15
	E–W/0.5	E–W/0.5/T3	E–W/0.5/T3/05
			E–W/0.5/T3/10
			E–W/0.5/T3/15
E–W/1.5	E–W/1.5/T1	E–W/1.5/T1/05	
		E–W/1.5/T1/10	
		E–W/1.5/T1/15	
E–W/1.5	E–W/1.5/T2	E–W/1.5/T2/05	
		E–W/1.5/T2/10	
		E–W/1.5/T2/15	
E–W/1.5	E–W/1.5/T3	E–W/1.5/T3/05	
		E–W/1.5/T3/10	
		E–W/1.5/T3/15	
E–W/3.0	E–W/3.0/T1	E–W/3.0/T1/05	
		E–W/3.0/T1/10	
		E–W/3.0/T1/15	
E–W/3.0	E–W/3.0/T2	E–W/3.0/T2/05	
		E–W/3.0/T2/10	
		E–W/3.0/T2/15	
E–W/3.0	E–W/3.0/T3	E–W/3.0/T3/05	
		E–W/3.0/T3/10	
		E–W/3.0/T3/15	

Thermal Comfort Simulations (iii): ENVI-Met Inputs

The scenario modeling and the thermal simulations are done with Envi-met version 4.3.2 (ENVI-MET Company, Essen, Germany). Envi-met is chosen for this simulation not only for its user-friendly interface, but also for its capacity to build 3d tree models even considering differences in canopy shape and density and size. The scenario modeling in Envi-met necessitates the street 3d models including the tree and monitoring points (receptors), the weather data, and human body parameters.

The street models are built according to the scenarios defined in Table 4. The typical street is set as 20 m large and 100 m long, corresponding to the average dimensions of the streets in the study area (Figure 1). The Figure 9 shows examples of street 3d models where trees, buildings and receptors are included. The height of the buildings are determined by the aspect ratio (Height/width). The trees are modeled in respect of their canopy shape, density and size. See the following figure (Figure 10) for the models of the three types of trees (T1, T2, and T3). The receptors are placed both sides of the streets (Figure 11), within 4 m away from the buildings and separated 10 m–12 m away from each other on each side; for comparability among the simulation results, their positions are maintained the same for all scenarios.

Since the purpose of the simulation is to measure the effects of tree configuration coupled with aspect ratio and orientation, the building and soil materials are set as default and the same for all scenarios. Thus, the variations of building and soil materials from one street to another are not included in the model in order to ensure that they do not interfere with the measurement of the “target effects”. Default unsealed soil is set for the ground material; concrete slab (hollow blocks) and tile roofing is set as default materials for all buildings.

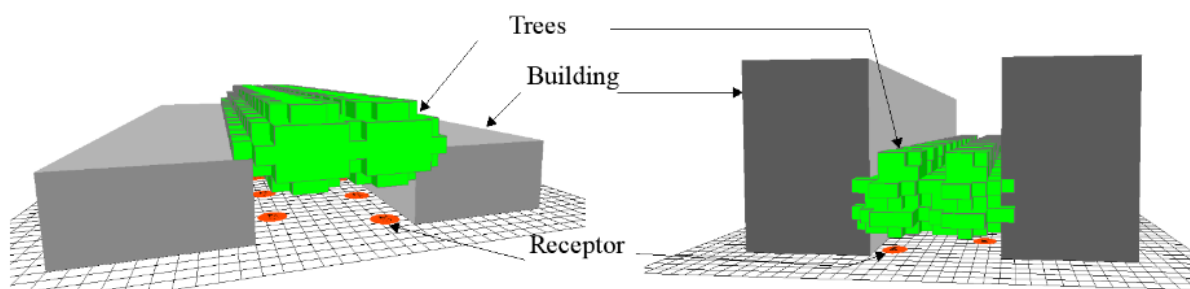


Figure 9. Examples of street 3d model in Envi-met V4.3.2.

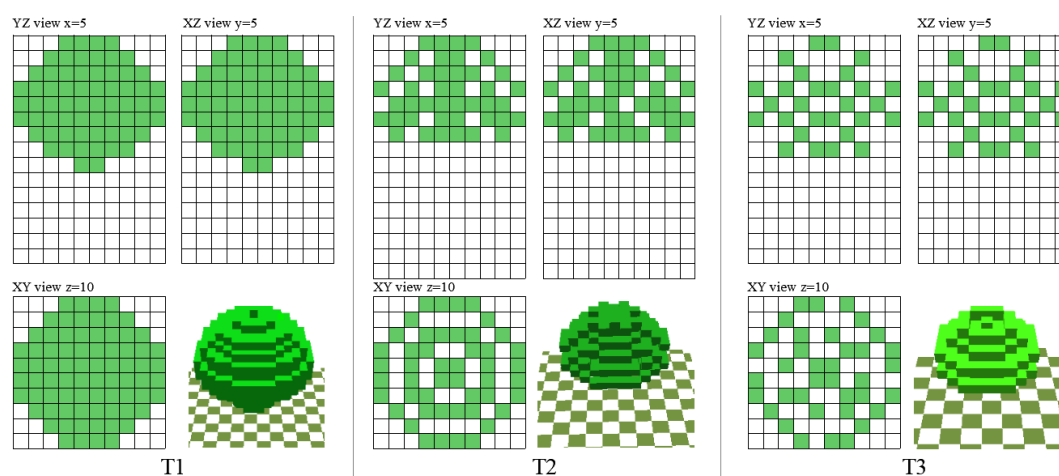


Figure 10. T1, T2 and T3 3d models showing different canopy shapes and densities.

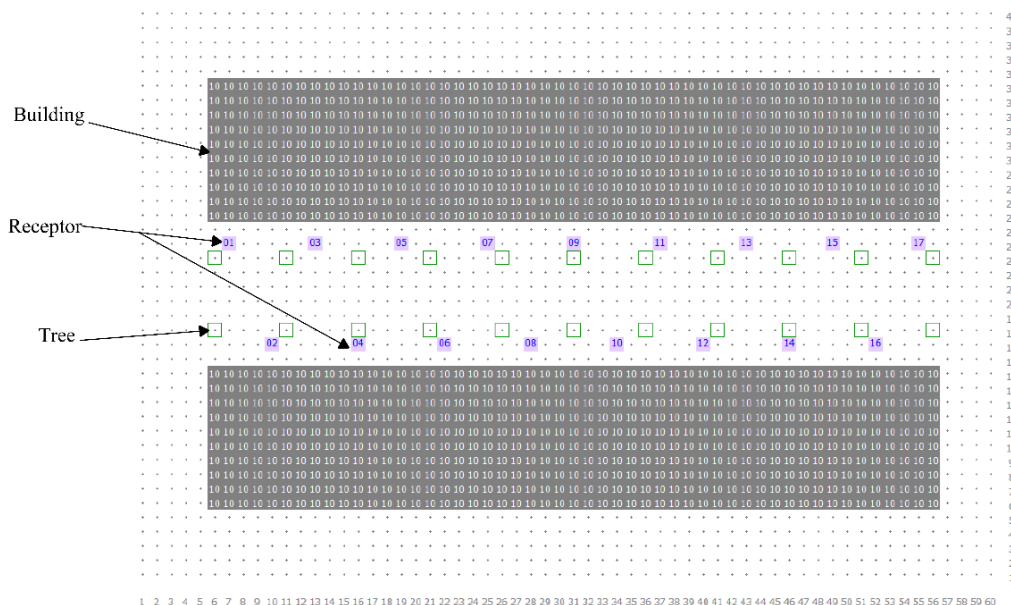


Figure 11. Receptors and tree layout.

The meteorological conditions comprise the wind speed, the wind direction, the roughness length at measurement site, the initial temperature of atmosphere (T), the specific humidity at 2500 m and the relative humidity (q). The wind speed is set as 3.3 m/s (calculated average from the meteorological data in Table 2). The wind direction is set as 244.5° from north (calculated average from the wind direction data presented in Table 5).

Table 5. Wind direction data between 0:00 and 23:00.

Time (h:mm)	0:00	1:00	2:00	3:00	4:00	5:00	6:00	7:00	8:00	9:00	10:00	11:00
wind direction (°)	219	213	261	276	282	287	286	273	75	288	293	289
Time (h:mm)	12:00	13:00	14:00	15:00	16:00	17:00	18:00	19:00	20:00	21:00	22:00	23:00
wind direction (°)	290	290	284	148	299	298	270	100	250	212	213	172

Data source: China standard climate monitoring station No 59316 (Shantou city).

Complementary to the wind speed, the roughness length defines the surface roughness at the location, where the wind speed was measured [62]; here, the roughness length is set as default in Envi-met (0.01), corresponding to the roughness of a typical urban area. The Envi-met default value is also used for the specific humidity at 2500 m (7.0 g/kg). For the temperature and the relative humidity (rH), simple forcing is used by inputting the temperature and relative humidity data—from 00:00 to 23:00—retrieved from the station No 59316 on the 8 July 2016 (see Figure 12).

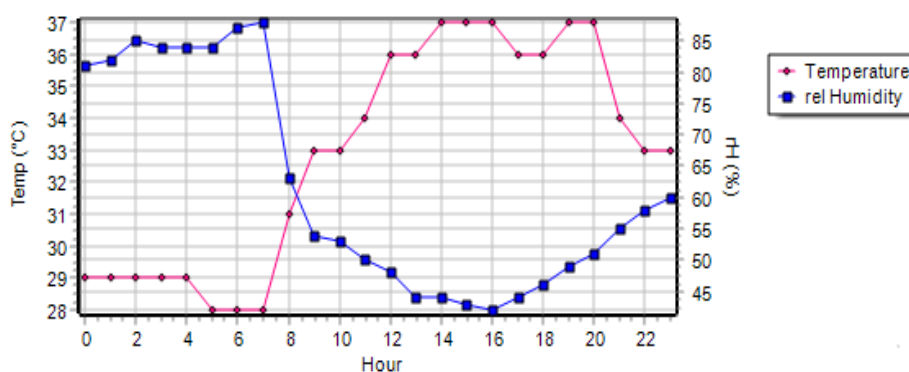


Figure 12. Background temperature and relative humidity simple forcing in Envi-met.

For the calculation of PMV, Human body parameters (age, gender, weight, height and surface area) are needed along with clothing insulation and metabolic rate. These parameters are set as described earlier in Section 2.3. The work metabolism is calculated as 80.21 W (for the Envi-met default walk speed of 1.21 m/s). The basal metabolism rate is 84.49 W, which gives a total metabolic rate of 164.70 W (=86.32 W/m²).

Output Analysis and Street Tree Guidelines (iv)

The simulations outputs (temperature, wind speed, and PMV) of the various scenarios will be on the one hand compared with the outputs of the reference scenarios where no tree is included in the model to show the relative effects of the street trees. On the other hand, the outputs of different scenarios will be compared with each other to determine the optimal cases.

In the next section, the outputs will be analyzed at 15:00—the hottest moment of the day, and at 1.5 m height. Air temperature and wind speed variations according to different scenarios will be analyzed; the PMV computed for 17 receptors (included in the models), through a “stage by stage” comparison, will help select the optimal tree configuration (tree type and layout distance). Heat Mitigation Rate (HMR) will be evaluated to see the contribution of the optimal vegetation configuration to the overall thermal comfort.

3. Results

The results analysis consists of comparing the simulation maps as follow: under a given AR, the effects of three sample trees (T1, T2, T3) on the wind speed and the air temperature are compared. For each sample tree the variation of the effects according to the trees interval (d) is also analyzed. Furthermore, the PMV values computed for each scenarios will be compared to identify the effects of each tree configuration parameter on heat mitigation.

3.1. Wind Speed

The wind speed maps (Figure 13) globally show that the ventilation in the street increases as the AR increases; this is noticeable for the reference maps (Ref. AR = 0.5, Ref. AR = 1.5, and Ref. AR = 3.0) as for the scenarios. Take T1 scenarios with d = 5 for instance, when the AR is 0.5 (scenario E-W/0.5/T1/05), the wind speed in the middle of the street ranges between 0.50 m/s and 1.00 m/s; when the AR is 1.5 (scenario E-W/1.5/T1/05), the wind speed in the same area increases between 1.25 m/s and 2.00 m/s and when the AR is 3.0 (scenario E-W/3.0/T1/05), it neatly goes beyond 1.75 m/s.

The comparison between the reference wind speed maps and the scenario wind speed maps—when T1, T2 and T3 are included—show that street trees influence the wind speed. In general, the trees have a decreasing effect on the average wind speed—likely because of the obstacle that the tree canopies constitute. Nevertheless, some local differences are also noticeable in terms of effects that the trees have on the street ventilation, especially at the “wind inlet”, depending on the AR. Here, the simulations are run with south-west winds and the streets are east-west oriented; the wind inlet is thus at the western opening of the street models. At the wind inlets, the ventilation is increased when the AR = 0.5—the trees (15 m–17 m) are higher than the buildings (10 m)—and the area covered by wind speeds above 2.00 m/s is more important than in the reference models where there is no tree. The opposite effect is observable when the AR = 3.0—the trees (15 m–17 m) are lower than the buildings (60 m): the area covered by wind speeds above 2.00 m/s is less than in the reference model.

It is also observable that T1 (with higher canopy density) provides a better ventilation under the canopy (at 1.5 m height, in this case) than T2 and T3 (medium and open canopy densities); but comparing the wind speed maps of scenarios with the same AR and tree, it is observable that the interval between the trees does not significantly influence the wind speed.

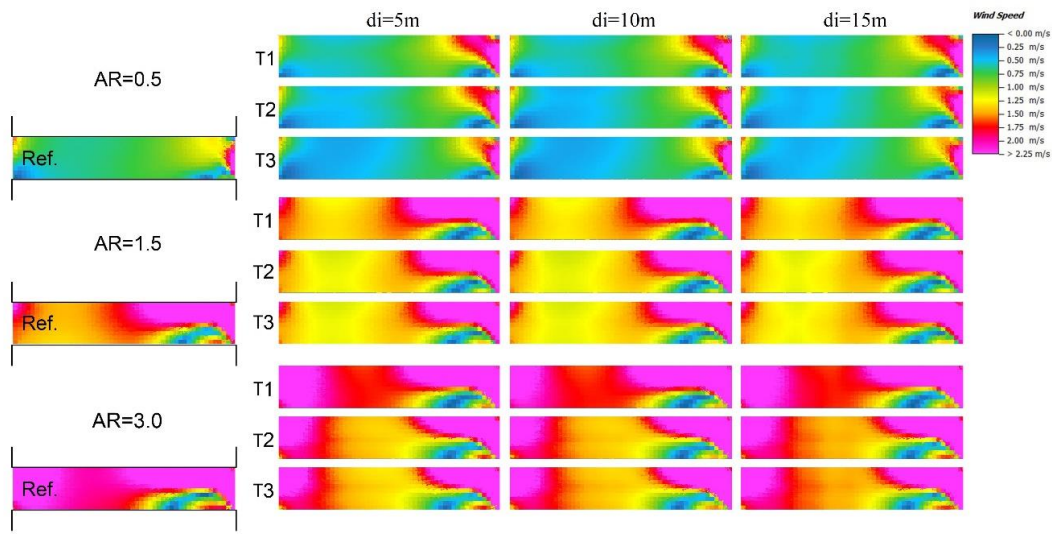


Figure 13. Wind speed maps at 1.5 m, comparing reference models and scenarios.

3.2. Air Temperature

The air temperature map (Figure 14), either by comparing the reference maps with different aspect ratios or by comparing scenarios with the same tree configuration but different aspect ratios, confirms the observation that higher AR have a heat mitigation effect at pedestrian level (the same observation has been made in the STCD analysis). For instance, the global temperature of the scenario E–W/0.5/T1/05 (AR = 0.5) is higher than that of the scenario E–W/1.5/T1/05 (AR = 1.5) which is also higher than that of the scenario E–W/3.0/T1/05 (AR = 3.0).

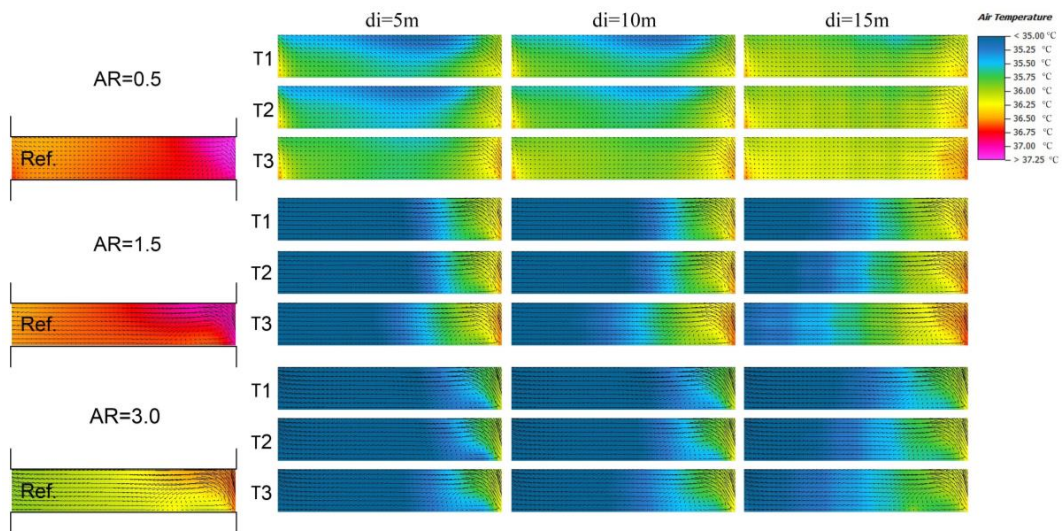


Figure 14. Air temperature maps at 1.5 m, comparing reference models and scenarios.

Besides, the comparison between the reference maps and the scenario maps under the same AR, globally confirms the cooling effect that tree has on the air temperature at pedestrian level. But specifically, different tree configurations have different levels of heat mitigation effect; in all cases, T1 has a better effect than T2 and T2 also has a better effect than T3. This steady increase of cooling effect of the trees—form T1 to T2 and T3—is likely due to the canopy density, which also follows a likewise decrease from T1 to T2 and T3 while the sizes of the three sample trees does not represent that much of a difference. Remembering, that the canopy is dense for T1, medium for T2 and open for T3, one can deduce that the denser the tree canopy is, the lower the air temperature at pedestrian

level is. But one can also observe that the interval between the trees influence the effect of the trees on the air temperature. Globally, the air temperature increases as the interval increases, which implies that the cooling effect of the street trees are higher when the trees are closer. This observation might be explained by the sky view factor [63–67] on the streets which increases as the interval between the trees increases, allowing more solar access on the street.

3.3. Predicted Mean Vote

Based on the previous analysis of wind speed air temperature maps, one can expect that T1 would have a better effect on thermal comfort which would be steadily increased as the trees are displayed at smaller intervals and furthered by higher aspect ratios. This could be confirmed through the quantitative analysis of the physiological sensation of thermal comfort at the receptor points using PMV data.

The PMV computed for the 17 receptors input in the simulation models are compared stage by stage, to quantify the physiological sensation of thermal comfort in different cases and detect the optimum tree configurations. First, are compared the effects of T1, T2 and T3 when planted at the same interval, under the same aspect ratio to detect the optimum tree type. Then, the effect of the optimum tree type is measured when planted at different intervals under the same aspect ratio; this second stage of comparison will help detect which interval is appropriate for an optimum comfort. Third, the heat mitigation rate of the optimum tree configuration (type and interval)—evaluated by percentage decrease of PMV—is analyzed under different aspect ratios.

The following radar chart (Figure 15) present the PMV values calculated for at the 17 receptors when AR = 0.5. PMV is compared for T1, T2 and T3 when di = 5 m (a), when di = 10 m (b) and when di = 15 m (c). The three charts show that scenarios with T1 always have lower PMV values regardless of the interval. The same conclusion can be drawn when the same comparison is made changing the AR (see Figure 16 when AR = 1.5 and Figure 17 when AR = 3.0).

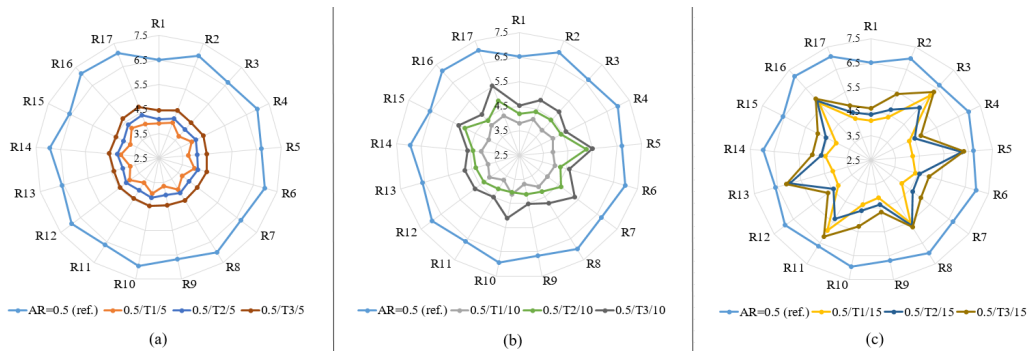


Figure 15. PMV variation according to Ti when AR = 0.5: (a) when di = 5 m; (b) when di = 10 m; (c) when di = 15 m.

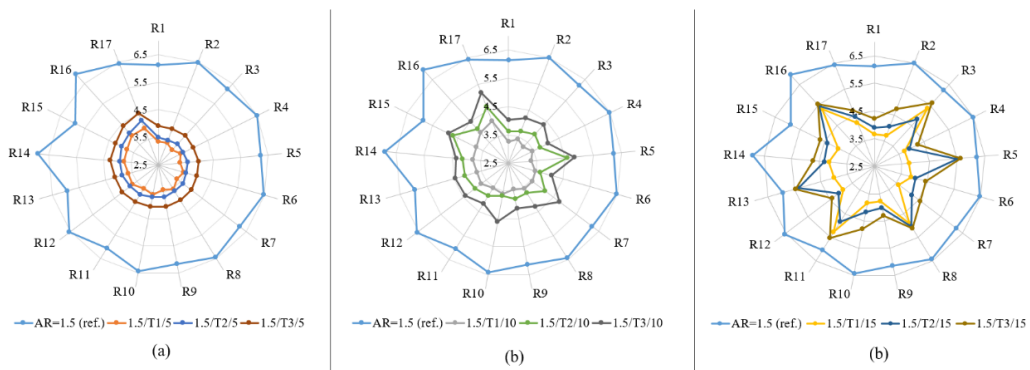


Figure 16. PMV variation according to Ti when AR = 1.5: (a) when di = 5 m; (b) when di = 10 m; (c) when di = 15 m.

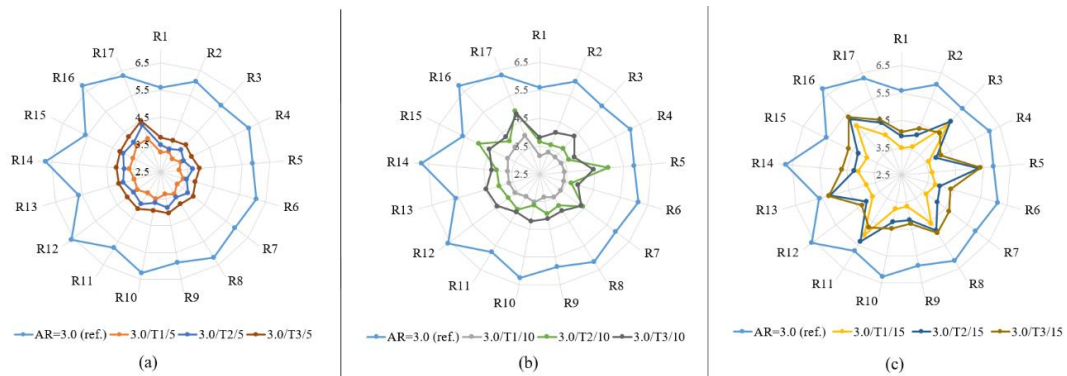


Figure 17. PMV variation according to T_i when $AR = 3.0$: (a) when $d_i = 5$ m; (b) when $d_i = 10$ m; (c) when $d_i = 15$ m.

Next, the effects of T_1 at different intervals are compared. As shown in Figure 18, one can globally observe that the closer the trees are, the lower the PMV gets (which means cooler temperatures are obtained under the canopies). Precisely, one can notice that the change of interval from d_{15} ($d_i >$ crown width) to d_{10} ($d_i =$ crown width) has a relatively significant impact on the heat mitigation, but a change from d_{10} to d_5 ($d_i <$ crown width) does not further the heat mitigation significantly. This observation which is confirmed even when the AR changes (see Figure 18a when the $AR = 0.5$, Figure 18b when $AR = 1.5$ and Figure 18c when $AR = 3.0$) can lead to deduce that the street trees have an optimum effect when they are planted at an interval equivalent to their crown width. Closer than that they have a slightly more but not that important of an effect. Furthermore, it is also shown that when the AR is higher, the PMV values are lower due to the influence that high aspect ratios have on the air temperature as described in Section 3.2. Based on this two-fold correlation of thermal comfort with both AR and trees interval, one can conclude that the T_1 planted at 5 m intervals has the best effect when the aspect ratio is 3.0, which makes E–W/3.0/ T_1 /05 the best heat-mitigating scenario, but because T_1 has close to that same efficiency when planted at 10 m intervals, it can be considered more economic; E–W/3.0/ T_1 /10 can thus be considered as the optimum scenario.

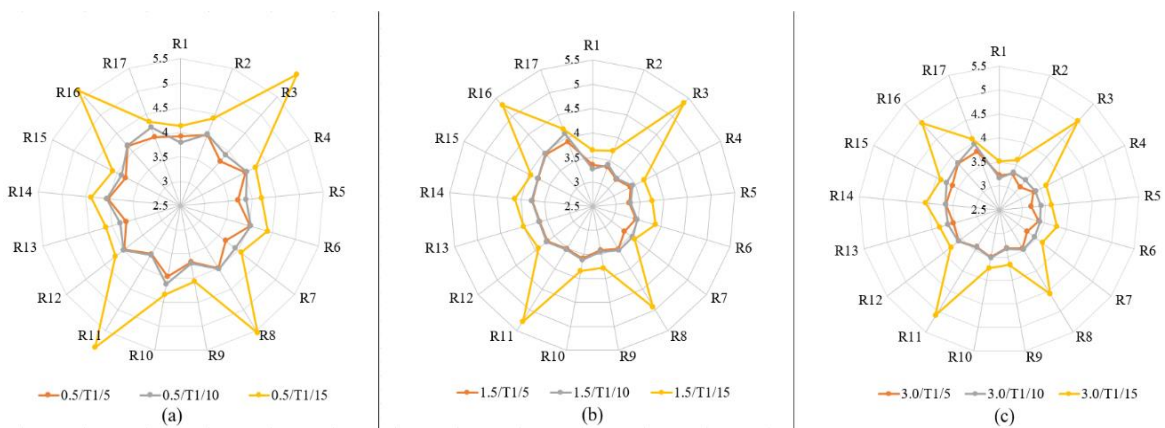


Figure 18. PMV variation according to d_i : (a) when $AR = 0.5$; (b) when $AR = 1.5$; (c) when $AR = 3.0$.

3.4. Heat Mitigation Rate (HMR)

Even though $T_1/10$ is considered as an optimum tree configuration because of the combined effects of the tree and the aspect ratio, this conclusion does not tell the exact share of contribution of $T_1/10$ in each AR case. To measure that, here is introduced the Heat Mitigation Rate (σ), estimated by calculating the percentage decrease of PMV between the reference models and the scenarios under the same AR (see the following Equation (1)).

$$\sigma_{ref-sc} = \frac{(PMV_{reference} - PMV_{scenario})}{PMV_{reference}} \times 100. \tag{1}$$

Since no tree is included in the reference models, the percentage decrease of PMV reflects exclusively the effect of the tree. The HMRs estimated for T1/d10 and presented in the following chart (Figure 19) globally show two different situations: one from the wind-inlet to the middle of the streets (from R1 to R9) and the other from the middle to the wind-outlet of the streets (from R10 to R17). Close to the wind-inlet, the optimum tree configuration has a higher mitigation rate in the south (even-numbered receptors) when the aspect ratio is low (AR = 0.5), while the same tree configuration has a better effect in the north (odd-numbered receptors) when the aspect ratio is medium (AR = 1.5) or high (AR = 3.0). From the middle to the wind-outlet of street, the optimum tree configuration has a neatly better HMR when the aspect ratio is medium. On the one hand, this can be explained by the correlation between the aspect ratio, the sky view factor and the solar access. Indeed, the lower the aspect ratio is, the higher the sky view factor is and the greater the solar access is, inducing more heat stress in the street [67]. Besides, the wind speed is lower in a street of a low AR than in a street of a higher AR. In such an unfavorable condition of a low AR (in this case AR = 0.5), even the optimum tree configuration has a better heat mitigation contribution when the AR is medium (1.5) or high (3.0). Nevertheless, when the AR is high, the default contribution of the buildings to the heat mitigation (less solar access and more wind speed) is so important, that the effect of the trees are not as significant as in a medium AR case. In consequence, T1/10 has a higher heat mitigation rate in a street when the AR is medium (1.5 in this case); but E-W/3.0/T1/10 is still considered as the optimum scenario (Figure 20) because of the overall and comprehensive comfort level provided by the buildings and the tree. This helps understand that even an optimum tree configuration has different heat mitigation rates in different street configurations cases, and definitely, both parameters (tree configuration and street configuration) are complementary for a better heat mitigation at pedestrian level, especially under extreme thermal conditions in summer.

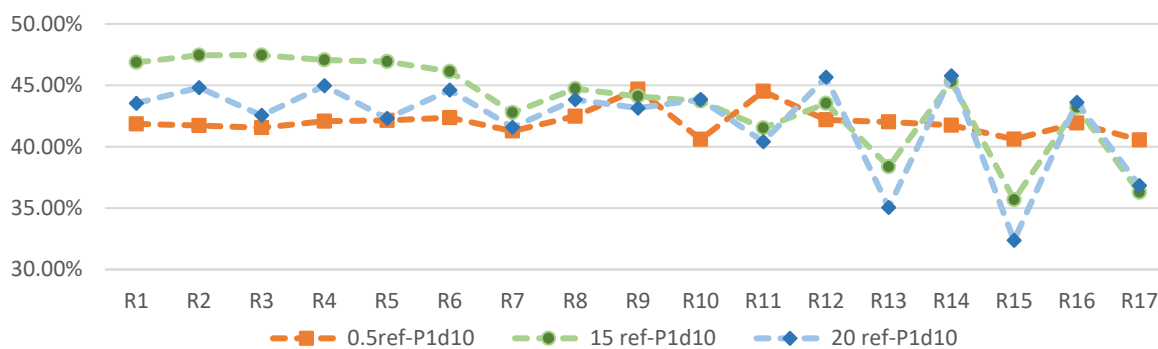


Figure 19. Heat mitigation rate of T1/d10 in different AR cases.



Figure 20. PMV values of P1/d10 in different AR cases.

3.5. Summary and Discussions

The street orientation, the aspect ratio, the canopy density density of trees and the interval between the trees are the four street design related parameters analysed in this study. As resulting from the STCD analysis, the orientation appears to be have an important influence on thermal comfort, which confirms the observation of many other studies [68–72]. The east–west oriented streets are observed as the most uncomfortable cases while the north-south orientation is the least problematic, which observation aligns itself with the majority of previous studies carried out on the effect of street orientation and explained by the prolonged period of solar exposure during summer. [22,73,74]. Here, the same observation as many other studies is made, showing the aspect ratio as a determinant parameter in street thermal comfort [73,75–79]; the higher it is the lower the temperature in the street canyon is at summer time. Nevertheless, the STCD analysis, besides the common observations, has shown a limit to the influence of aspect ratio and orientation. When the natural climatic conditions are very hot (PMV values in this case are above +3 between 8:00 and 19:00), the effect of street orientation and the aspect ratio are far from enough to provide thermal comfort at pedestrian level.

The canopy density and the layout interval are the two tree configuration parameters considered in this study. The canopy density, what is expressed in other studies as the Leaf area Index (LAI) is shown as very important parameter determining the cooling effect of trees. Montague and Kjelgren defined the LAI as “a dimensionless value of the leaf area per unit of ground area” [60]. Here, the tree sample with a dense canopy (T1) has a better cooling effect than those with a medium (T2) or an open canopy (T3). This variance in the effect is due to the lower level of radiant heat and lower amount of terrestrial radiation beneath the canopy when the canopy density is higher [59,61]. But more importantly, The STCO analysis has contributed by showing that the interval of layout does not make any important difference in the variation of the wind speed, but significantly influences the air temperature in the street and consequently the efficiency of street trees. Actually, the cooling effect of trees at pedestrian level is observed as optimum when the interval between the trees equals their crown width.

The main contribution of this paper resides in examining the combined behaviors of all the above mentioned parameters. The results show that even though the effects of the individual parameters are confirmed, the effect of their combination on reducing heat stress is not as linear as expected. For instance, a higher canopy density and a higher aspect ratio are each expected to reduce heat stress but when combined, even the tree with higher canopy density planted at the optimal interval has the highest heat mitigation rate on medium-aspect-ratio streets (AR = 1.5) but a higher aspect ratio does not reduce much of the overall heat sensation.

For urban practitioners, this conclusion could means that tree configuration is complementary to street configuration and vice-versa as thermal comfort at pedestrian level is concerned. Not only the tree type (especially the canopy density) and the layout have to be selected carefully, but the street aspect ratio should also be adjusted (when possible) in order to obtain the best possible street thermal comfort. To that end, the analytical framework proposed by this paper can be applied to any other study area. At a planning stage, the framework can also be used to test the efficiency of any species intended for street planting.

4. Conclusions

In this paper, street tree configuration—defined by the tree type and the tree layout—is studied in terms of the effects they have on heat mitigation at pedestrian level (1.5 m–1.75 m) when combined with various street configuration—defined by the orientation and the aspect ratio. In order to detect which tree type and layout is optimal for heat mitigation in extreme summer conditions, even in the worst street configuration case, an analytical framework is proposed, composed of two main parts: a Spatial–Temporal Comfort Diagnosis—intended to identify the street configurations the least favorable for thermal comfort—and a Street Thermal Comfort Optimization—where different tree

configurations are tested with the least favorable street configurations to evaluate their contributions to heat mitigation.

The analytical framework is applied to a historical site named Xiaogongyuan, the “small park” in Shantou city, China. The STCD—which estimated the Psychologically Equivalent Temperature between 9:00 and 19:00 for the 24 combinations of aspect ratio and orientation identified in the study area—demonstrated that, under an extreme summer condition, the heat stress is uncomfortable in all cases regardless of the streets’ orientations and the aspect ratios and that the east–west oriented streets are the most uncomfortable cases.

When the east–west orientation is considered with three aspect ratios (AR = 0.5, AR = 1.5 and AR = 3.0) and combined with 9 sample tree configurations (mainly defined by the canopy density and the interval of layout), the STCO analysis confirms the importance of canopy density in the cooling effect of trees. The STCO analysis also shows that the interval of layout influences significantly the efficiency of street tree. Actually, the effect of trees on the thermal comfort at pedestrian level is optimum when the interval between the trees equals their crown width (10 m in this case); when the trees are more distant than that, the street gets hotter, and when they are closer than that, the improvement of thermal comfort is not significant.

The Heat Mitigation Rate estimated for the optimum tree configuration (T1/d10), when applied to different aspect ratios, shows that street tree configuration—even the optimum one—can have a higher or a lower efficiency in terms of contribution to heat mitigation depending on the aspect ratio of the street they are planted on.

In the case of “small park” regarding the conclusions of the STCO, *mangifera indica* (T1) is recommended as street tree among the common tree species and should be planted with 10 m intervals. Other species could be used also, but should meet the requirement of a high canopy density and the interval of layout should not be more than the crown width. The future planning schemes of the area, should also consider increasing the building height on streets with low aspect ratios; ideally, a minimum AR of 1.5 is recommended especially on east–west oriented streets.

Since the analytical model has been tested with the east–west orientation, these specifications are more imperative for east–west oriented street but considering that, as shown in the STCD analysis, the east–west orientation is the least favorable in terms of default thermal conditions, the optimum tree and street configurations recommended in this case are potentially efficient for other orientations (NE–SW, NW–SE, and NS). Nevertheless, the analytical model, as demonstrated, can be applied to other orientations and aspect ratios (even asymmetrical cases) for any specific case studies. Here it has been observed that the street tree can have a higher Heat Mitigation Rate more on one side of the street than the other depending on the aspect ratio and the street orientation in relation to the dominant wind direction. The one-side or axial tree planting can be added as a parameter to the scenario design to compare the effects of other tree layouts as well.

Author Contributions: Conceptualization, B.Z., K.B.B. and J.Z.; methodology, K.B.B.; validation, B.Z., J.Z.; formal analysis, K.B.B.; investigation, B.Z., J.Z. and G.W.; resources, B.Z., J.Z. and G.W.; data curation, K.B.B.; writing—original draft preparation, K.B.B.; writing—review and editing, K.B.B.; visualization, K.B.B.; supervision, B.Z.; project administration, B.Z.; funding acquisition, B.Z.

Funding: This research was funded by the Natural Science Foundation of China, grant number 51478470.

Acknowledgments: The authors would like to thank Yiling Wang (postgraduate student at the School of Architecture and Art, Central South University, Changsha) for his helps provided during the data curation.

Conflicts of Interest: The authors declare no conflict of interest.

References

1. Emmanuel, M.R. *An Urban Approach to Climate-Sensitive Design: Strategies for the Tropics*; Taylor & Francis: London, UK, 2005.
2. Solomon, S. *Climate Change 2007: The Physical Science Basis: Working Group I Contribution to the Fourth Assessment Report of the IPCC*; Cambridge University Press: Cambridge, UK, 2007.

3. Johansson, E.; Thorsson, S.; Emmanuel, R.; Krüger, E. Instruments and methods in outdoor thermal comfort studies—The need for standardization. *Urban Clim.* **2014**, *10*, 346–366. [[CrossRef](#)]
4. Ahmad, K.; Khare, M.; Chaudhry, K.K. Wind tunnel simulation studies on dispersion at urban street canyons and intersections—A review. *J. Wind Eng. Ind. Aerodyn.* **2005**, *93*, 697–717. [[CrossRef](#)]
5. Vardoulakis, S.; Fisher, B.E.; Pericleous, K.; Gonzalez-Flesca, N. Modelling air quality in street canyons: A review. *Atmos. Environ.* **2003**, *37*, 155–182. [[CrossRef](#)]
6. Ali-Toudert, F.; Mayer, H. Numerical study on the effects of aspect ratio and orientation of an urban street canyon on outdoor thermal comfort in hot and dry climate. *Build. Environ.* **2006**, *41*, 94–108. [[CrossRef](#)]
7. Rodríguez Algeciras, J.A.; Consuegra, L.G.; Matzarakis, A. Spatial-temporal study on the effects of urban street configurations on human thermal comfort in the world heritage city of Camagüey-Cuba. *Build. Environ.* **2016**, *101*, 85–101. [[CrossRef](#)]
8. Lamarca, C.; Qüense, J.; Henríquez, C. Thermal comfort and urban canyons morphology in coastal temperate climate, Concepción, Chile. *Urban Clim.* **2018**, *23*, 159–172. [[CrossRef](#)]
9. Silva, J.P. Solar radiation and street temperature as function of street orientation. An analysis of the status quo and simulation of future scenarios towards sustainability in Bahrain. In *E3S Web of Conferences*; EDP Sciences: Les Ulis, France, 2017; Volume 23, p. 02002.
10. Qaid, A.; Ossen, D.R. Effect of asymmetrical street aspect ratios on microclimates in hot, humid regions. *Int. J. Biometeorol.* **2014**, *59*, 657–677. [[CrossRef](#)] [[PubMed](#)]
11. ASHRAE. *ANSI/ASHRAE Standard 55-2013, Thermal Environmental Conditions for Human Occupancy*; ASHRAE: Atlanta, GA, USA, 2013.
12. Freire, R.Z.; Oliveira, G.H.C.; Mendes, N. Predictive controllers for thermal comfort optimization and energy savings. *Energy Build.* **2008**, *40*, 1353–1365. [[CrossRef](#)]
13. Korkas, C.D.; Baldi, S.; Michailidis, I.; Kosmatopoulos, E.B. Occupancy-based demand response and thermal comfort optimization in microgrids with renewable energy sources and energy storage. *Appl. Energy* **2016**, *163*, 93–104. [[CrossRef](#)]
14. He, S.; Yang, X. Coupling relationship between summer microclimate and spatial layout of street canyons in the white stupa temple area of Beijing. *J. Landsc. Res.* **2018**, *10*, 83–89. [[CrossRef](#)]
15. Givoni, B. Impact of planted areas on urban environmental quality: A review. *Atmos. Environ. Part B Urban Atmos.* **1991**, *25*, 289–299. [[CrossRef](#)]
16. Gill, S.; Handley, J.; Ennos, A.; Pauleit, S. Adapting cities for climate change: The role of the green infrastructure. *Built Environ.* **2007**, *33*, 115–133. [[CrossRef](#)]
17. Fahmy, M.; Sharples, S.; Yahiya, M. LAI based tree selection for mid latitude urban developments: A micro climatic study in Cairo, Egypt. *Build. Environ.* **2010**, *45*, 345–357. [[CrossRef](#)]
18. Wong, N.H.; Yu, C. Study of green areas and urban heat island in a tropical city. *Habitat Int.* **2005**, *29*, 547–558. [[CrossRef](#)]
19. Akbari, H.; Pomerantz, M.; Taha, H. Cool surfaces and shade trees to reduce energy use and improve air quality in urban areas. *Sol. Energy* **2001**, *70*, 295–310. [[CrossRef](#)]
20. Picot, X. Thermal comfort in urban spaces: Impact of vegetation growth: Case study: Piazza della Scienza, Milan, Italy. *Energy Build.* **2004**, *36*, 329–334. [[CrossRef](#)]
21. Jamei, E.; Rajagopalan, P.; Seyedmahmoudian, M.; Jamei, Y. Review on the impact of urban geometry and pedestrian level greening on outdoor thermal comfort. *Renew. Sustain. Energy Rev.* **2016**, *54*, 1002–1017. [[CrossRef](#)]
22. Ali-Toudert, F.; Mayer, H. Effects of asymmetry, galleries, overhanging façades and vegetation on thermal comfort in urban street canyons. *Sol. Energy* **2007**, *81*, 742–754. [[CrossRef](#)]
23. Lin, B.; Li, X.; Zhu, Y.; Qin, Y. Numerical simulation studies of the different vegetation patterns' effects on outdoor pedestrian thermal comfort. *J. Wind Eng. Ind. Aerodyn.* **2008**, *96*, 1707–1718. [[CrossRef](#)]
24. Shashua-Bar, L.; Tsiros, I.X.; Hoffman, M.E. A modeling study for evaluating passive cooling scenarios in urban streets with trees: Case study—Athens, Greece. *Build. Environ.* **2010**, *45*, 2798–2807. [[CrossRef](#)]
25. Shashua-Bar, L.; Tsiros, I.X.; Hoffman, M.E. Passive cooling design options to ameliorate thermal comfort in urban streets of a Mediterranean climate (Athens) under hot summer conditions. *Build. Environ.* **2012**, *57*, 110–119. [[CrossRef](#)]
26. Andreou, E. Thermal comfort in outdoor spaces and urban canyon microclimate. *Renew. Energy* **2013**, *55*, 182–188. [[CrossRef](#)]

27. Coutts, A.M.; White, E.C.; Tapper, N.J.; Beringer, J.; Livesley, S.J. Temperature and human thermal comfort effects of street trees across three contrasting street canyon environments. *Theor. Appl. Climatol.* **2016**, *124*, 55–68. [CrossRef]
28. Bowler, D.E.; Buyung-Ali, L.; Knight, T.M.; Pullin, A.S. Urban greening to cool towns and cities: A systematic review of the empirical evidence. *Landsc. Urban Plan.* **2010**, *97*, 147–155. [CrossRef]
29. Ivana, V.B.; Dragan, D.M.; Stevan, M.S. Evaluation and improvement of outdoor thermal comfort in urban areas on extreme temperature days: Applications of automatic algorithms. *Build. Environ.* **2015**, *94*, 632–643. [CrossRef]
30. Dragan, D.M.; Ivana, V.B.; Stevan, M.S. Influence of changing trees locations on thermal comfort on street parking lot and footways. *Urban For. Urban Green.* **2017**, *23*, 113–124. [CrossRef]
31. Van Hoof, J.; Mazej, M.; Hensen, J.L. Thermal comfort: Research and practice. *Front. Biosci.* **2010**, *15*, 765–788. [CrossRef]
32. Höppe, P. The physiological equivalent temperature—A universal index for the biometeorological assessment of the thermal environment. *Int. J. Biometeorol.* **1999**, *43*, 71–75. [CrossRef] [PubMed]
33. Chen, Y.C.; Matzarakis, A. Modified physiologically equivalent temperature—Basics and applications for western European climate. *Theor. Appl. Climatol.* **2018**, *132*, 1275–1289. [CrossRef]
34. Ye, G.; Yang, C.; Chen, Y.; Li, Y. A new approach for measuring predicted mean vote (PMV) and standard effective temperature (SET*). *Build. Environ.* **2003**, *38*, 33–44. [CrossRef]
35. Blazejczyk, K.; Jendritzky, G.; Broede, P.; Fiala, D.; Havenith, G.; Epstein, Y.; Psikuta, A.; Kampmann, B. An introduction to the Universal Thermal Climate Index (UTCI). *Geogr. Pol.* **2013**, *86*, 5–10. [CrossRef]
36. Fröhlich, D.; Matzarakis, A. *RayMan Manual Version 0.1*; Research Centre Human Biometeorology, German Meteorological Service: Freiburg, Germany, 2017.
37. Matzarakis, A.; Rutz, F.; Mayer, H. Modelling radiation fluxes in simple and complex environments: Basics of the RayMan model. *Int. J. Biometeorol.* **2010**, *54*, 131–139. [CrossRef] [PubMed]
38. Ozkeresteci, I.; Crewe, K.; Brazel, A.J.; Bruse, M. Use and evaluation of the Envi-met model for environmental design and planning: An experiment on linear parks. In Proceedings of the 21st International Cartographic Conference, Durban, South Africa, 10–16 August 2003. Available online: <https://pdfs.semanticscholar.org/b74e/913b1d0b54269ed5e661238b428c1ad671e2.pdf> (accessed on 2 November 2018).
39. National Bureau of Statistics. China City Statistical Yearbook 2016. Available online: <http://www.yearbookchina.com/navibooklist-N2017060038-1.html> (accessed on 24 August 2018).
40. Geiger, R. “Klassifikation der Klimate nach W. Köppen” [Classification of Climates after W. Köppen]. *Landolt-Börnstein—Zahlenwerte und Funktionen aus Physik, Chemie, Astronomie, Geophysik und Technik, alte Serie*; Springer: Berlin, Germany, 1954; Volume 3, p. 603.
41. Geiger, R. *Überarbeitete Neuauflage von Geiger, R.: Köppen-Geiger/Klima der Erde*; (Wandkarte 1:16 Mill.); Klett-Perthes: Gotha, Germany, 1961.
42. Weatherbase. Shantou, China. Available online: <https://www.weatherbase.com/weather/weather-summary.php3?s=61395&cityname=Shantou,+China> (accessed on 24 August 2018).
43. China Ground Climate Data International Exchange Station Data Set Station Information. Available online: http://www.360doc.com/document/12/0123/21/8088674_181500436.shtml (accessed on 24 August 2018).
44. Höppe, P. Heat balance modelling. *Experientia* **1993**, *49*, 741–746. [CrossRef] [PubMed]
45. VDI. *Methods for the Human Biometeorological Evaluation of Climate and Air Quality for the Urban and Regional Planning. Part I: Climate*; VDI Guideline 3787; Part 2; Beuth: Berlin, Germany, 1998.
46. Fanger, P.O. *Thermal Comfort*; McGraw-Hill Book Company: New York, NY, USA, 1972; p. 244.
47. Gagge, A.P.; Fobelets, A.P.; Berglund, P.E. A standard predictive index of human response to the thermal environment. In Proceedings of the ASHRAE Annual Meeting, Portland, OR, USA, 22 June 1986.
48. Matzarakis, A.; Rutz, F.; Mayer, H. Estimation and calculation of the mean radian temperature within urban structures. In *Biometeorology and Urban Climatology at the Turn of the Millennium*; Dera, R.J., Kalma, J.D., Oke, T.R., Auliciems, A., Eds.; Selected Papers from the Conference ICB-ICUC99, WCASP-50, WMO/TD No. 1026; World Meteorological Organization: Geneva, Switzerland, 2000; pp. 273–278.
49. Spagnolo, J.; de Dear, R. A field study of thermal comfort in outdoor and semi-outdoor environments in subtropical Sydney Australia. *Build. Environ.* **2003**, *38*, 721–738. [CrossRef]
50. Gulyas, A.; Unger, J.; Matzarakis, A. Assessment of the microclimatic and human comfort conditions in a complex urban environment: Modelling and measurements. *Build. Environ.* **2006**, *41*, 1713–1722. [CrossRef]

51. Wang, Y.; Bakker, F.; de Groot, R.; Wortche, H.; Leemans, R. Effects of urban trees on local outdoor microclimate: Synthesizing field measurements by numerical modelling. *Urban Ecosyst.* **2015**, *18*, 1305–1331. [[CrossRef](#)]
52. Zheng, T.; Kevin, K.L.; Edward, N. Urban tree design approaches for mitigating daytime urban heat island effects in a high-density urban environment. *Energy Build.* **2016**, *114*, 265–274. [[CrossRef](#)]
53. Hwang, R.-L.; Lin, T.-P.; Matzarakis, A. Seasonal effects of urban street shading on long-term outdoor thermal comfort. *Build. Environ.* **2011**, *46*, 863–870. [[CrossRef](#)]
54. International Standardization Organization. ISO 7730: Ergonomics of the Thermal Environment—Analytical Determination and Interpretation of Thermal Comfort Using Calculation of the PMV and PPD Indices and Local Thermal Comfort Criteria. 2005. Available online: <https://www.iso.org/standard/39155.html> (accessed on 15 September 2018).
55. Matzarakis, A.; Mayer, H. Another Kind of Environmental Stress: Thermal Stress. WHO Collaborating Centre for Air Quality Management and Air Pollution Control. *Newsletters* **1996**, *18*, 7–10.
56. Matzarakis, A.; Mayer, H.; Iziomon, M. Applications of a universal thermal index: Physiological equivalent temperature. *Int. J. Biometeorol.* **1999**, *43*, 76. [[CrossRef](#)] [[PubMed](#)]
57. Memon, R.A.; Leung, D.Y.; Liu, C.H. Effects of building aspect ratio and wind speed on air temperatures in urban-like street canyons. *Build. Environ.* **2010**, *45*, 176–188. [[CrossRef](#)]
58. Fang, H.; Xin, R.; Xiao, Z. Selection and Deployment of Tree Species for Urban Road Afforestation in Shantou City. *J. Chin. Urban For.* **2008**, *6*, 32–33.
59. Kotzen, B. An investigation of shade under six different tree species of the Negev desert towards their potential use for enhancing micro-climatic conditions in landscape architectural development. *J. Arid Environ.* **2003**, *55*, 231–274. [[CrossRef](#)]
60. Montague, T.; Kjelgren, R. Energy balance of six common landscape surfaces and the influence of surface properties on gas exchange of four containerized tree species. *Sci. Hortic.* **2004**, *100*, 229–249. [[CrossRef](#)]
61. Shahidan, M.F.; Shariff, M.K.; Jones, P.; Salleh, E.; Abdullah, A.M. A comparison of *Mesua ferrea* L. and *Huracrepitans* L. for shade creation and radiation modification in improving thermal comfort. *Landsc. Urban Plan.* **2010**, *97*, 168–181. [[CrossRef](#)]
62. ENVI-met. A1. Configuration File: Basic Settings. Available online: <http://www.envi-met.info/documents/onlinehelpv3/hs60.htm> (accessed on 24 August 2018).
63. Johnson, D. Urban modification of diurnal temperature cycles in Birmingham, UK. *J. Climatol.* **1985**, *5*, 221–225. [[CrossRef](#)]
64. Yamashita, S.; Sekine, K.; Shoda, M.; Yamashita, K.; Hara, Y. On relationships between heat island and sky view factor in the cities of Tama River basin, Japan. *Atmos. Environ. (1967)* **1986**, *20*, 681–686. [[CrossRef](#)]
65. Unger, J. Intra-urban relationship between surface geometry and urban heat island: Review and new approach. *Clim. Res.* **2004**, *27*, 253–264. [[CrossRef](#)]
66. Svensson, M.K. Sky view factor analysis—Implications for urban air temperature differences. *Meteorol. Appl.* **2004**, *11*, 201–211. [[CrossRef](#)]
67. Yan, H.; Fan, S.; Guo, C.; Wu, F.; Zhang, N.; Dong, L. Assessing the effects of landscape design parameters on intra-urban air temperature variability: The case of Beijing, China. *Build. Environ.* **2014**, *76*, 44–53. [[CrossRef](#)]
68. Kleerekoper, L.; van Esch, M.; Salcedo, T.B. How to make a city climate-proof, addressing the urban heat island effect. *Resour. Conserv. Recycl.* **2012**, *64*, 30–38. [[CrossRef](#)]
69. Yang, F.; Qian, F.; Lau, S.S. Urban form and density as indicators for summer time outdoor ventilation potential: A case study on high-rise housing in Shanghai. *Build. Environ.* **2013**, *70*, 122–137. [[CrossRef](#)]
70. Givoni, B. *Urban Design in Different Climates*; World Meteorological Organization: Geneva, Switzerland, 1989.
71. Herrmann, J.; Matzarakis, A. Mean radiant temperature in idealised urban canyons—Examples from Freiburg, Germany. *Int. Biometeorol.* **2012**, *56*, 199–203. [[CrossRef](#)] [[PubMed](#)]
72. Mills, G. Urban climatology and urban design. In Proceedings of the 15th International Congress of Biometeorology and International Conference on Urban Climatology, Sydney, Australia, 8–12 November 1999.
73. Johansson, E. Influence of urban geometry on outdoor thermal comfort in a hot dry climate: A study in Fez, Morocco. *Build. Environ.* **2006**, *41*, 1326–1338. [[CrossRef](#)]
74. Krüger, E.; Pearlmutter, D.; Rasia, F. Evaluating the impact of canyon geometry and orientation on cooling loads in a high-mass building in a hot dry environment. *Appl. Energy* **2010**, *87*, 2068–2078. [[CrossRef](#)]

75. Ahmed, K. A comparative analysis of the outdoor thermal environment of the urban vernacular and the contemporary development: Case studies in Dhaka. In Proceedings of the 11th PLEA International Conference on Architecture of the Extremes, DeadSea, Israel, 3–8 July 1994; pp. 3–8.
76. Emmanuel, R.; Johansson, E. Influence of urban morphology and sea breeze on hot humid microclimate: The case of Colombo, Sri Lanka. *Clim. Res.* **2006**, *30*, 189–200. [[CrossRef](#)]
77. Nunez, M. The Energy Balance of an Urban Canvas. Ph.D. Thesis, University of British Columbia, Vancouver, BC, Canada, 1974.
78. Oke, T.R. Canyon geometry and the nocturnal urban heat island: Comparison of scale model and field observations. *J. Climatol.* **1981**, *1*, 237–254. [[CrossRef](#)]
79. Holmer, B. A simple operative method for determination of sky view factors in complex urban canyons from fish eye photographs. *Meteorol. Z.* **1992**, *1*, 236–239. [[CrossRef](#)]



© 2018 by the authors. Licensee MDPI, Basel, Switzerland. This article is an open access article distributed under the terms and conditions of the Creative Commons Attribution (CC BY) license (<http://creativecommons.org/licenses/by/4.0/>).